Clays and Clay Minerals, Vol. 56, No. 6, 612–621, 2008.

STACKING FAULTS WITH 180º LAYER ROTATION IN CELADONITE, AN Fe- AND Mg-RICH DIOCTAHEDRAL MICA

TOSHIHIRO KOGURE[1], JUN KAMEDA[1], AND VICTOR A. DRITS[2]

[1] Department of Earth and Planetary Science, Graduate School of Science, The University of Tokyo, 7-3-1 Hongo, Bunkyo-ku, Tokyo, 113-0033, Japan

[2] Geological Institute of the Russian Academy of Sciences, Pyzhevsky per 7, 119017 Moscow, Russia

Abstract—Stacking disorder in celadonite, a dioctahedral mica with Fe and Mg as major octahedral cations and which generally adopts the 1*M* stacking sequence, was investigated mainly by using transmission electron microscopy (TEM). The selected-area electron diffraction patterns with 0*kl* reflections along the [100] beam direction correspond to the 1*M* stacking but those along the [110], [1$\bar{1}$0], [010], [310], and [3$\bar{1}$0] directions are frequently streaked along the [001]* direction or contain extra spots from twinned domains. Three-dimensional stacking analyses using sets of two high-resolution TEM images along different directions of the same area of one crystal indicate that all stacking faults involve only 180º layer rotations. These stacking faults produce greater peaks of 0*kl* reflections than expected in powder X-ray diffraction (XRD) patterns. Simulation of the XRD patterns indicated that 180º layer rotations occur at >10% of total interlayer regions in one celadonite specimen. The interlayer region of celadonite is characterized by a near-zero ditrigonal rotation angle, a small surface corrugation of the basal oxygen plane, and a small amount of Al substitution in the tetrahedral sheets. These features suggest that there is no preference for any of the six stacking angles around the interlayer region. The abundance of 180º layer rotation rather than ±60º and ±120º in the present specimens may be related to their ribbon-like morphologies elongated along the *a* axis.

Key Words—Celadonite, Electron Microscopy, Mica, Polytype, Stacking Faults, X-ray Diffraction.

INTRODUCTION

Polytypism is a common phenomenon in many phyllosilicates. Polytypism of micas, in particular, has been investigated extensively, both experimentally and theoretically, but is not yet fully understood. Polytypism of micas may be described as the rotation between adjacent layers, the angle of which is restricted to a multiple (n) of 60º about the c* axis. Polytypes with layer rotations of $2n60º$ (subfamily A) occur more frequently than those of $(2n+1)60º$ (subfamily B). This is primarily explained by the atomic configuration of the interlayer region of micas (*e.g.* Ferraris and Ivaldi, 2002). However, the occurrence of subfamily B polytypes, although uncommon, is not rare. Lepidolite often occurs as the $2M_2$ polytype with ±60º rotations (*e.g.* Levinson, 1953), and several illite specimens adopt the $2M_2$ configuration (Threadgold, 1959; Drits *et al.*, 1966; Zhukhlistow *et al.*, 1973; Slonimskaya *et al.*, 1978). The origins of the $2M_2$ polytype in lepidolite were discussed in previous works (*e.g.* Takeda *et al.*, 1971; Brigatti *et al.*, 2005). Furthermore, the 2*O* polytype with 180º rotation occurs in anandite from Sri Lanka (Giuseppetti and Tadini, 1972) and in phlogopite (Ferraris *et al.*, 2001).

* E-mail address of corresponding author:
kogure@eps.s.u-tokyo.ac.jp
DOI: 10.1346/CCMN.2008.0560602

Stacking faults in micas have origins similar to the structural variables that produce polytypes, but they are not periodic and occur at a unit-layer scale. An effective technique to investigate the stacking faults or long-period polytypes is high-resolution transmission electron microscopy (HRTEM) (*e.g.* Iijima and Buseck, 1978; Baronnet, 1992; Kogure and Nespolo, 1999a, 1999b). Kogure and his coworkers (Kogure and Nespolo, 1999a; Kogure and Bunno, 2004; Kameda *et al.*, 2007) reported the occurrence of stacking faults with $(2n+1)60º$ rotations in various micas. Kogure and Nespolo (1999a), in particular, found that stacking faults that involve various rotation angles exist in a $2M_1$-dominant Mg-rich annite in granite. They employed a 'three dimensional stacking analysis' using a set of two HRTEM images along the X_i direction and the Y_i direction where X_i is, for example, [100], [110], or [1$\bar{1}$0] and Y_i is [010], [310], or [3$\bar{1}$0] in the 1*M* and $2M_1$ polytypes (Bailey, 1984). Interstratification of $2n60º$ and $(2n+1)60º$ rotations was also reported in lepidolite (Kogure and Bunno, 2004) and in magnesian illite (gümbelite) (Kameda *et al.*, 2007); both sets of authors used HRTEM.

The analyses of stacking faults in layer minerals by XRD methods is difficult because stacking errors only broaden reflections or change several reflections to a 'band.' However, XRD studies are enhanced when computer simulation of the experimental XRD patterns is used. Comparison of calculated positions, intensities, and profiles with observed reflections provides an

estimate of the content and distribution of stacking errors (*e.g.* Drits and Tchoubar, 1990). For example, Sakharov *et al*. (1990) found that in glauconite mica layers involving $2n60^\circ$ and $(2n+1)60^\circ$, layer rotations occur with equal probability, but layers with different orientations are generally segregated. Studies by McCarty and Reynolds (1995), Cuadros and Altaner (1998a, 1998b), and Ylagan *et al*. (2000) on illite-smectite showed that stacking faults involving layer rotations of $2n60^\circ$ and $(2n+1)60^\circ$ were found to occur.

Celadonite is an Fe^{3+}-rich dioctahedral mica containing similar amounts of Fe^{2+} and/or Mg^{2+} at the octahedral sites (Rieder *et al*., 1999), and it commonly adopts the 1*M* polytype (Buckley *et al*., 1978). Although celadonite is commonly impure and fine-grained, and therefore difficult to study, Zhukhlistov *et al*. (1977), Zhukhlistov (2005), and Tsipursky and Drits (1986) refined the structure of celadonite using oblique-texture electron diffraction.

Kogure *et al.* (2007) examined unheated and heat-treated celadonite and found that celadonite-1*M* generally contains frequent stacking faults. Surprisingly, they found that all faults involve the layer rotation of 180º only. The present paper describes the observation of the faults by HRTEM, the powder XRD patterns and their simulation, and possible origins for these stacking faults.

MATERIALS AND METHODS

Three celadonite specimens were investigated: from Taiheizan, Akita, Japan (Kimbara and Shimoda, 1973); from Krivoi Rog, Ukraine (Zhukhlistov *et al.*, 1977); and from Zaval'e, Pobuj'e, Ukraine (Malkova, 1956; Tsipursky and Drits, 1986). The reported formulae are:

Taiheizan:
$(K_{0.817}Na_{0.176})(Al_{0.159}Fe^{3+}_{1.066}Fe^{2+}_{0.140}Mg_{0.666})(Si_{3.721}Al_{0.279})O_{10}(OH)_2$

Krivoi Rog:
$(K_{0.83}Na_{0.01}Ca_{0.04})(Al_{0.05}Fe^{3+}_{1.15}Fe^{2+}_{0.36}Mg_{0.41}Ti_{0.01})(Si_{3.94}Al_{0.06})O_{10}(OH_{1.99}F_{0.01})$

Zaval'e:
$(K_{0.89}Ca_{0.10})(Al_{0.05}Fe^{3+}_{0.96}Fe^{2+}_{0.26}Mg_{0.73})(Si_{3.94}Al_{0.06})O_{10}(OH)_2$

The Taiheizan specimen contains more Al at the octahedral and tetrahedral sites than the other two specimens.

Each specimen for TEM examination was prepared following the method proposed by Kogure (2002). In short, powder was embedded in epoxy resin between two glass slides. After hardening, the glass slides were cut using a diamond wheel to laths of ~1 mm thick. The laths were thinned to ~50 μm by mechanical grinding and then argon ion milled. Examination by HRTEM was performed at 200 kV using a JEOL JEM-2010 UHR with a nominal point resolution of 2.0 Å. The HRTEM images were captured on film or using a Gatan MSC 794 bottom-mounted CCD camera; they were taken at sufficiently thin regions of the specimen, and by adjusting the defocus value, to record the contrast that corresponds to the projected potential of the crystal structure (Kogure, 2002). Noisy contrast from amorphous materials in HRTEM images was removed using a Wiener-filter (Marks, 1996; Kilaas, 1998) developed by K. Ishizuka (HREM Research, Inc.) and implemented using a Gatan DigitalMicrograph version 3.10.0.

Powder XRD patterns were collected using a Rigaku RINT-Ultima$^+$ diffractometer with CuKα radiation, a graphite monochromator, a 0.3 mm receiving slit, and 0.5º divergence and anti-scatter slits. A continuous scan rate of $1^\circ 2\theta$ min^{-1} was adopted. Simulation of powder XRD patterns was performed using *DIFFaX* (Treacy *et al.*, 1991) which calculates diffraction patterns from layered materials with various stacking sequences.

RESULTS

HRTEM analyses

Typical images (Figure 1a) of the Zaval'e celadonite crystals, dispersed on a microgrid with holey carbon film, revealed that the crystals have a lath- or ribbon-like morphology that is common for the three specimens investigated. Cross sections of the crystals (Figure 1b) showed them to be 50 to ~150 nm thick. Selected-area electron diffraction (SAED) patterns from the same area in a celadonite crystal, along the [100] (Figure 1c) and $[3\bar{1}0]$ (or [310]) (Figure 1d) directions, indicate that the stacking along [100] is 1*M* and well ordered because any streaking parallel to the c^* axis is below detection. In contrast, the pattern along the $[3\bar{1}0]$ direction (Figure 1d) contains extra spots on the 13*l* row, indicating the existence of twinned domains formed by mutual layer rotation with angles of $(2n+1)60^\circ$ (Kogure and Nespolo, 1999a). This apparent inconsistency between the two patterns suggests that stacking disorder involves 180º layer rotations in the 1*M* stacking sequence. The intralayer shift of the 2:1 layer along the $[\bar{1}00]$ direction for the 1*M* polytype changes to the [100] direction by a 180º layer rotation, which does not affect the diffraction pattern along the [100] direction.

The HRTEM image of the Krivoi Rog celadonite recorded along the [100] direction (Figure 2a) revealed that the stacking is uniform and no stacking faults are observed. In contrast, the HRTEM image of the same area, but along the $[3\bar{1}0]$ (or [310]) direction (Figure 2b), shows several stacking faults. The white bar in each 2:1 layer connects the closest dark spots in the lower and upper tetrahedral sheets. These bars are slanted by $\pm a/6$. The symbol '+' and '−' at the bottom indicates the direction of the slant of the white bar in each layer; '+' for the bar diagonally down ($+a/6$) and '−' diagonally up ($-a/6$). This slant corresponds to the direction of the projection of the intralayer shift in a 2:1 layer on the

https://doi.org/10.1346/CCMN.2008.0560602 Published online by Cambridge University Press

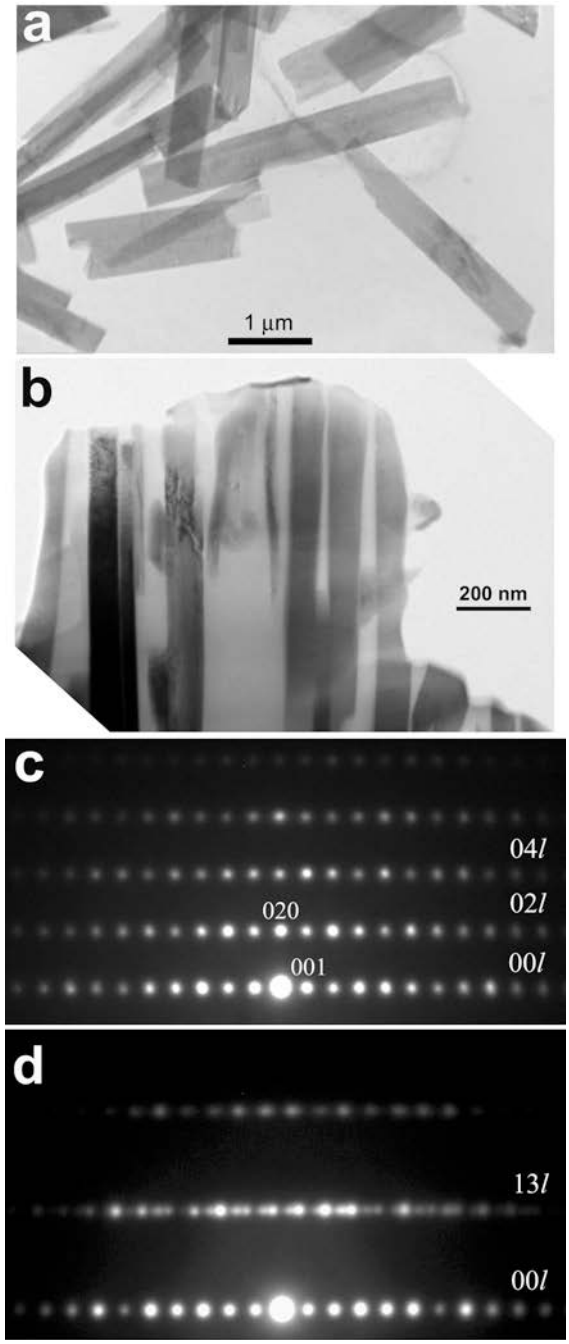

Figure 1. (a) Bright-field image of Zaval'e celadonite, showing a lath- or ribbon-like morphology with the (001) surface and elongation along the *a* axis. (b) Bright-field image of the cross-sectional specimen used for selected-area electron diffraction (SAED) and HRTEM. The material between the crystals is epoxy resin embedded during preparation of the sample. (c) SAED pattern from a crystal in (b), with the beam direction parallel to the *a* axis of celadonite-1*M*. Note that the reflection rows are discrete with no streak. (d) SAED pattern from the crystal in (c) but the crystal is rotated by 30º about the *c** axis, showing extra spots which indicate twinned domains and mutual layer rotation at the twin boundaries with angles of $(2n+1)60^{\circ}$.

imaging plane (Baronnet and Kang, 1989). As described by Kogure and Bunno (2004), the sequence of different symbols ('+ −' or '− +') in the image along Y_i, *i.e.* along the [010], [310], and [3$\bar{1}$0] directions for the 1*M* polytype, indicates stacking with a rotation angle of $(2n+1)60^{\circ}$.

In Figure 2a, the contrast at the octahedral sheet in the 2:1 layer does not correspond to the expected contrast for the *trans*-vacant dioctahedral sheet that was identified by previous structure refinements (Zhukhlistov *et al*., 1977; Zhukhlistov, 2005; Tsipursky and Drits, 1986). This result occurs by cation migration induced by dehydroxylation. Kogure (2007) suggested that dioctahedral 2:1 phyllosilicates (muscovite, paragonite, pyrophyllite, *etc*.) are dehydroxylated by the electron beam radiation in a TEM. On the other hand, Tsipursky *et al*. (1985), Muller *et al*. (2000a, 2000b), and Drits *et al.* (1995) reported that cation migration from the *trans*-vacant dioctahedral arrangement to the *cis*-vacant arrangement occurs in celadonite by dehydroxylation with heating. From these results, the recorded structure in the HRTEM images is probably not *trans*-vacant dioctahedral as in the unheated celadonite. This phenomenon will be discussed further in a future study. However, this cation migration would not be expected to change the stacking sequence of the layers. In addition, the number of 2:1 layers recorded in Figure 2a is smaller than that in Figure 2b, although the same area was recorded. This result is related to radiation damage. The images in Figure 2b were recorded prior to the specimen being rotated by 30º about the *c** axis to record Figure 2a. Beam damage before recording Figure 2a destroyed a few layers at the right and left edges of the packet, resulting in an amorphous region. Thus, making the correspondence of layers between the two images in Figure 2 is difficult. Nevertheless, stacking faults in Figure 2b must be contained in the area shown in Figure 2a, although they do not appear in the image. This result requires a rotation angle of 180º at the faults.

Another example of the three-dimensional stacking analysis is shown in Figure 3. The beam direction in Figure 3a is [110] or [1$\bar{1}$0] of the 1*M* polytype. Stacking faults are observed in this image and in Figure 3b. As for Figure 2b, the orientation of each layer was determined from image contrast and denoted as '+' or '−' symbols at the bottom of Figures 3a and 3b (the degree of slant in Figure 3a is $\pm b/6$). The 2:1 layers indicated by the black arrow (top right) in Figures 3a and 3b show a variation in contrast, the reason for which is not clear; the arrows are assumed to indicate identical layers. With this assumption, all layers recorded in the two images can be related to each other. By comparing the sequences of the '+' and '−' symbols in Figures 3a and 3b, the sign of each corresponding layer is reversed. Thus, for a symbol change of '+ −' (or '− +') at an interlayer in Figure 3b (this indicates $(2n+1)60^{\circ}$ as described above), the symbols at the corresponding interlayer are '− +' (or

https://doi.org/10.1346/CCMN.2008.0560602 Published online by Cambridge University Press

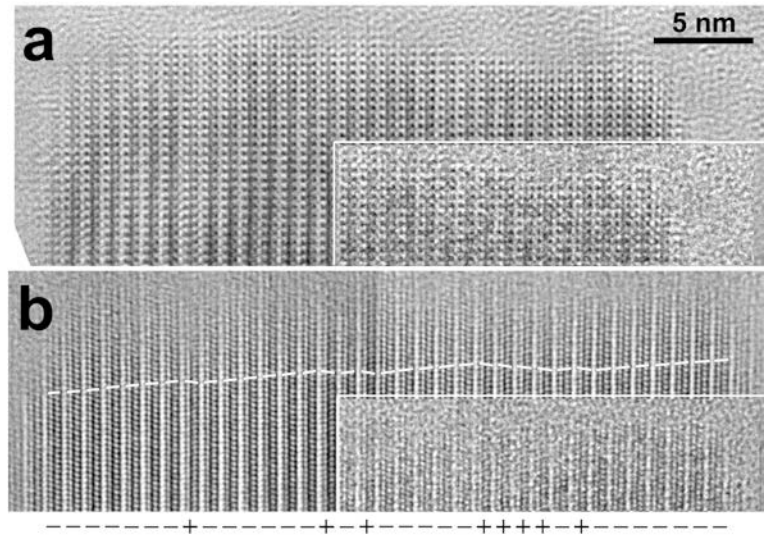

Figure 2. (a) Processed HRTEM image of a crystallite from Krivoi Rog celadonite recorded along the [100] direction. No stacking faults are observed. (b) Processed HRTEM image of the same region but the crystallite is rotated by 30º about the c^* axis. The white bar in each layer connects the two closest dark spots within the upper and lower tetrahedral sheets in a 2:1 layer, and the sign at the bottom of the figure indicates the slant direction of the bar. The inset at the bottom right of each figure shows the original, unprocessed HRTEM image.

'+ −') in Figure 3a. Figure 3c shows the sequence of signs across the interlayer with +60º and 180º rotations, if observed along various X_i and Y_i directions (the result with −60º rotation is just a flip of that with +60º rotation horizontally). Two arrows numbered 1 and 2 indicate the intralayer shift with the length of $a/3$, for a layer and the overlying layer. In this case, arrow 1 is set parallel to the $-X_1$ direction. The two symbols, *e.g.* '+ −', indicate how the two intralayer shifts are imaged in the HRTEM image along the X_i and Y_i directions. '0' indicates no slant for the bar, with the intralayer shift that is parallel or anti-parallel to the beam direction. In Figure 3c, the derivation of the symbols for Y_i directions requires an explanation. If the arrow (the intralayer shift) is perpendicular to the beam direction, the shift is imaged by the amount $a/3$. On the other hand, the periodicity of the projection for the 2:1 layer is $a/2$, owing to the C-centered unit cell. Consequently, the shift of $+a/3$ is apparently observed as $-a/6$ ($+a/3 - a/2$) in the HRTEM image recorded along the Y_i direction. Hence, the shift of $+a/3$ has the symbol '−'. The sequences of '+ −' and '− +' never appear along any X_i directions for +60º rotation but these sequences do appear for 180º. In conclusion, the stacking sequence in Figure 3 involves only 0º (1*M* stacking) and 180º layer rotations.

XRD analysis

Electron diffraction and three-dimensional stacking analyses using HRTEM for the three celadonite specimens showed identical results. However, the areas investigated by TEM are too limited to conclude that stacking faults with 180º rotation are common throughout the entire specimen. To overcome this limitation, the effect of stacking faults on the powder XRD pattern was simulated and compared to experimental patterns.

Simulations using *DIFFaX* are similar to that described by Kogure *et al.* (2006). According to the HRTEM results, each celadonite crystal was assumed to consist of two kinds of layers rotated by 180º from one another (this is equivalent to reversal of sign of the x coordinate of each atom in the orthogonal coordinate system). These two kinds of layers are expressed as layer A and layer B. The ratio of the numbers of the two kinds of layers in a crystal is defined as W_A and W_B and it is assumed that layer B is equal to or less than layer A ($W_B \leqslant W_A$). Next, the probability that layer B succeeds layer A is expressed as P_{AB}. Similarly P_{AA}, P_{BB}, and P_{BA} are defined to express the stacking. Of these six parameters, only two are independent because they have the following relations to each other:

$$W_A + W_B = 1,\ P_{AA} + P_{AB} = 1$$
$$P_{BA} + P_{BB} = 1,\ P_{AB} = (W_B/W_A)P_{BA} = (W_B/W_A)(1-P_{BB})$$

Among the six parameters, use of W_B and P_{BB} to express the stacking is sensible. With the assumption of $W_B \leqslant W_A$, P_{BB} can be changed from 0 to 1. If $P_{BB} = 1$, the two kinds of layers are completely segregated. If $P_{BB} = 0$, the stacking contains a maximum amount of 'ABA' sequence, *i.e.* without BB pairs. In the simulation, the atomic parameters for the Zaval'e celadonite (by Tsipursky and Drits, 1986) were used, and a pseudo-Voigt function (the same ratio of Gauss and Lorentz functions) with a full-width at the half maximum of 0.22º was assumed for the peak profile.

Figure 4a shows an example of the simulation where W_B was fixed at 1/3 and P_{BB} was varied from 0.0 to 1.0.

https://doi.org/10.1346/CCMN.2008.0560602 Published online by Cambridge University Press

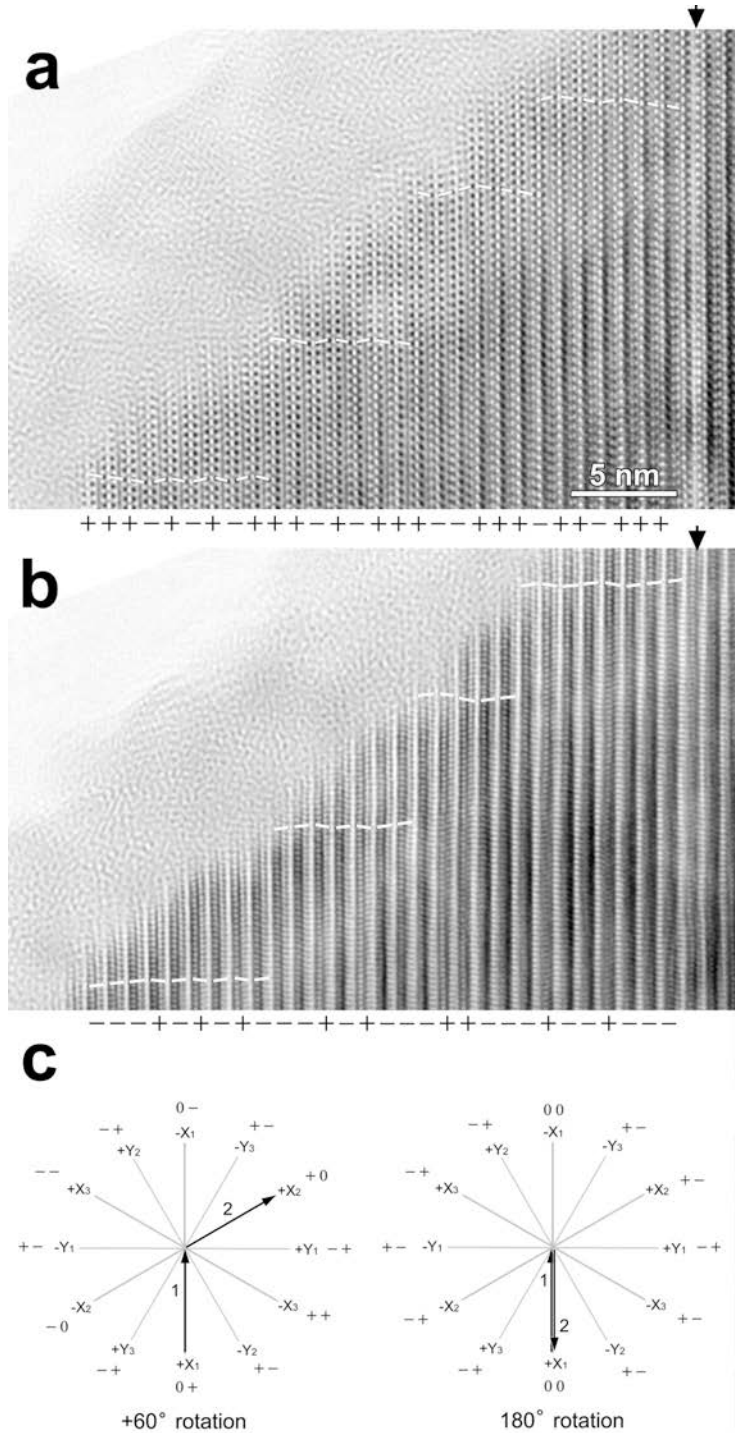

Figure 3. (a) Processed HRTEM image of a crystallite from Krivoi Rog celadonite recorded along the [110] or [$\bar{1}$10] direction. (b) Processed HRTEM image of the same crystal but with the crystallite rotated by 30º about the *c** axis. The layers indicated by the black arrows in both figures are regarded as identical, owing to their brighter contrast than others. (c) Diagrams showing how the 60º and 180º mutual rotation of the neighboring layers should be observed in the HRTEM images (see the text for details).

The value of 1/3 for W_B seems reasonable because the value is 0.23 and 0.31 in Figures 2 and 3, respectively, and it is 0.46 and 0.32 for the other two grains investigated using HRTEM. Figure 4b represents experimental powder diffraction patterns from the Taiheizan and Zaval'e specimens. The cell dimensions refined from a number of the peak positions in these diffraction patterns are shown in Table 1 with a list of the observed

https://doi.org/10.1346/CCMN.2008.0560602 Published online by Cambridge University Press

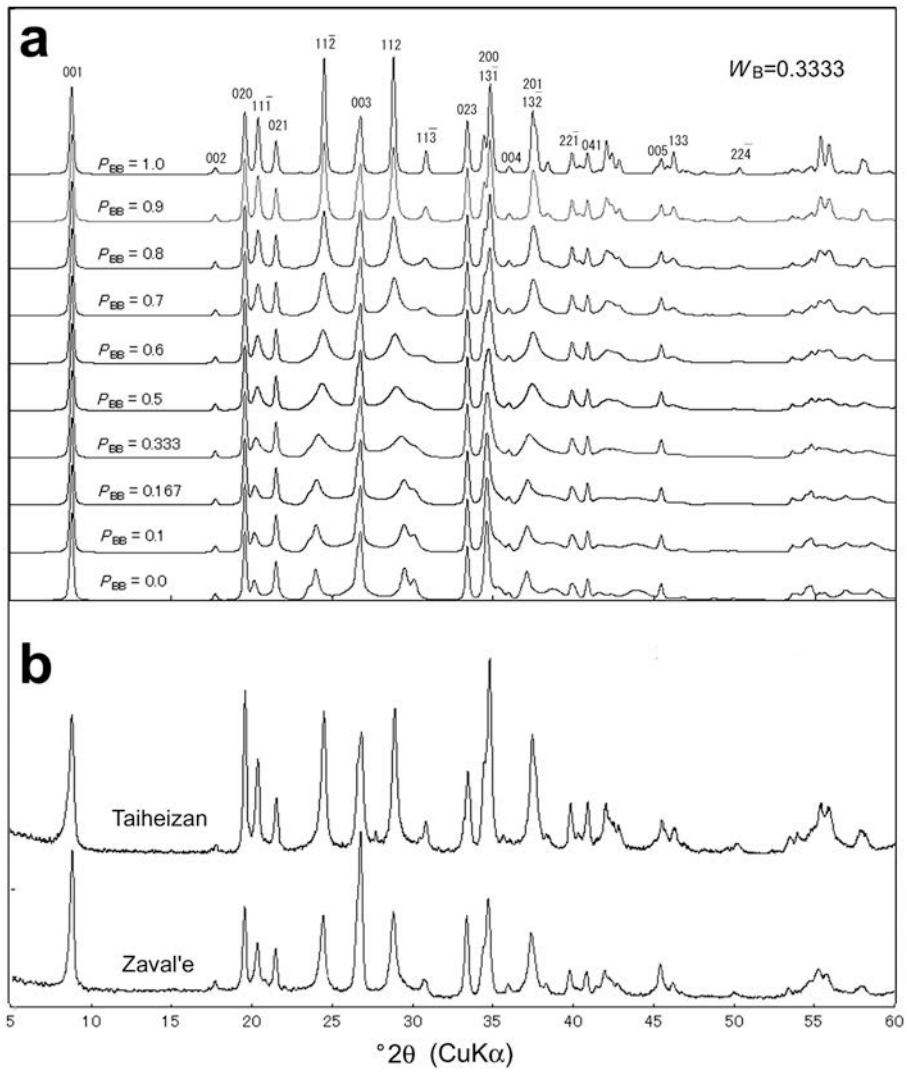

Figure 4. (a) Simulations of the powder XRD patterns from celadonite-1*M* containing the stacking faults with 180º stacking rotation, using the *DIFFaX* program. Parameters for the simulations, W_B and P_{BB} are explained in the text. (b) Experimental powder XRD patterns of celadonite from Taiheizan and Zaval'e.

and calculated *d* values for the typical peaks. The sample size of Krovoi Rog was too small to obtain sufficient diffraction intensity. Compared with the simulated pattern, where P_{BB} = 1.0, which is identical to the pattern for the fault-free 1*M* structure, the Zaval'e specimen shows a pattern characteristic of a structure which contains 180º stacking faults. Among peaks from 19 to 36º2θ, the peak heights of the 11$\bar{1}$, 11$\bar{2}$, 112, 11$\bar{3}$, and (13$\bar{1}$, 200) reflections are less than expected when compared to 020, 021, (022, 003), and 023 (the indices in parenthesis indicate peak overlap). If compared with simulated patterns with various P_{BB} values, the pattern from Zaval'e is close to that with P_{BB} = 0.8 (the largest peak for 003 may be due to preferred orientation). The ratio of the interlayer to form a 180º rotation is expressed as $W_A P_{AB} + W_B P_{BA}$. This value is 0.13 for W_B = 1/3 and P_{BB} = 0.8, indicating that >10% of the total interlayer regions are faulted with 180º rotation. On the other hand, the pattern of the Taiheizan specimen is close to the simulated pattern with P_{BB} = 0.9, suggesting more ordered stacking.

DISCUSSION

Some factors responsible for the stacking angle between adjacent layers in micas

The interlayer region in micas is partly determined by the ditrigonal symmetry of the tetrahedral sheets in the 2:1 layers. This symmetry is caused by the mutual rotation of adjacent tetrahedra in opposite directions around *c** by the angle α, the ditrigonal rotation angle. The angle α is determined by the misfit of the lateral dimensions between the octahedral and tetrahedral sheets. For instance, an increase in Fe and Mg in the

https://doi.org/10.1346/CCMN.2008.0560602 Published online by Cambridge University Press

Table 1. Refined cell dimensions from the powder XRD pattern, and observed and calculated peak positions.

hkl	— Taiheizan — $d_{obs.}$ (Å)	$d_{calc.}$ (Å)	—— Zavalé —— $d_{obs.}$ (Å)	$d_{calc.}$ (Å)
001	9.894	9.935	10.121	9.994
002	4.946	4.968	5.007	4.997
020	4.510	4.514	4.551	4.538
11$\bar{1}$	4.329	4.338	4.362	4.365
021	4.105	4.110	4.139	4.132
11$\bar{2}$	3.613	3.623	3.645	3.643
022	3.333	3.341	3.351	3.359
003	3.306	3.312	3.332	3.331
112	3.074	3.078	3.108	3.100
11$\bar{3}$	2.887	2.893	2.903	2.908
023	2.672	2.670	2.688	2.685
20$\bar{1}$	2.593	2.601	2.607	2.620
130		2.595		2.610
13$\bar{1}$	2.565	2.571	2.583	2.585
200		2.562		2.582
004	2.484	2.484	2.497	2.499
13$\bar{2}$	2.394	2.395	2.408	2.408
201		2.376		2.394
11$\bar{4}$	2.340	2.337	2.349	2.350
22$\bar{1}$	2.254	2.254	2.268	2.269
041	2.200	2.201	2.212	2.212
	a (Å)	5.216 (7)	*a* (Å)	5.254 (7)
	b (Å)	9.028 (9)	*b* (Å)	9.075 (9)
	c (Å)	10.114 (6)	*c* (Å)	10.170 (6)
	β (º)	100.78 (8)	β (º)	100.67 (9)

octahedral sheet and a decrease of Al in the tetrahedral sheets of the 2:1 layers in muscovite would accompany a decrease in α (*e.g.* Brigatti *et al*., 1998). The rotation of adjacent layers by (2*n*+1)60º should be less favorable because the pairs of the tetrahedral sheets across the interlayer region form a trigonal prism of oxygen atoms around K and create close superposition of the oxygen atoms vertically. However, the smaller the α angle, the smaller this disadvantage is, because the atomic arrangements with 2*n*60º and (2*n*+1)60º become similar. Hence, the small α is probably a requirement to form the rotation of (2*n*+1)60º. For instance, phlogopite-2*O* reported by Ferraris *et al*. (2001) has an α value of 2.13º. This value is considerably smaller than those in other micas. Simulation of experimental XRD patterns from illite-smectite with limited expandability is also in agreement with the α rotation discussed above (Drits *et al.*, 2006). The greater the amount of Fe and Mg in the octahedral sheet and the smaller the amount of Al in the tetrahedral sheet of the illite-like layers, the greater the probability of (2*n*+1)60º stacking faults, probably due to the decrease in α (Drits *et al.*, 2006).

In addition, the adjacent tetrahedra across the long edges of the *trans*-octahedral site are tilted and the bridging basal oxygen atoms between the tilted tetrahedra move further toward the middle of the layer by Δz with respect to the other basal oxygen atoms of each tetrahedron. As a result, the basal oxygen plane is corrugated. Δz is near zero for homo-octahedral micas (*i.e.* the same cations at the three sites in the octahedral sheet). In contrast, the value of Δz is larger for meso-octahedral micas (*i.e.* different cations at *trans*- and *cis*-sites) (Brigatti and Guggenheim, 2002; Ferraris and Ivaldi, 2002). *Trans*-vacant micas like muscovite are regarded as meso-octahedral. Among the six pairs of oxygen atoms across the interlayer region around K, the oxygen−oxygen distance for the two pairs formed by the depressed oxygen atoms are significantly larger than those for the other four pairs when the stacking angle is 0º or 180º. In contrast, the grooves formed by the rows of the depressed oxygen atoms are rotated with respect to each other in the adjacent layer and therefore each depressed atom has a non-depressed atom as a pair across the interlayer when the stacking angle is ±60º or ±120º. As a result, the distances in the six pairs are equalized significantly and the repulsion between the nearest oxygen atoms across the interlayer would be expected to be less. Thus, it is consistent that muscovite with large α and Δz values mainly adopts the $2M_1$ polytype with ±120º layer rotations.

Finally, the amount of Al substituting for Si in the tetrahedral sheets may affect the stacking angles. This substitution changes the lateral dimension of the tetrahedral sheet and α as a consequence. Furthermore, substitution of Al for Si in the tetrahedral sheets leads to an undersaturated charge on the basal oxygen atoms, so that they have a tendency to repel each other. Thus, the influence of α and Δz is probably enhanced by large amounts of Al substitution.

Structural features of celadonite-1M

The crystal structure of the two celadonite samples, Zaval'e and Krivoi Rog, were refined by Tsipursky and Drits (1986) and Zhukhlistov (2005), respectively, using oblique-texture electron diffraction (OTED). According to the structural formulae, the negative layer charge in both structures is located in the octahedral sheets. The tetrahedral sheets have the same cation composition (0.06 atoms of Al per $O_{10}(OH)_2$). Therefore, the interlayer arrangements in both structures are nearly identical. For Zaval'e, α = 0.54º, Δz = 0.030 Å, <Si,Al−O> = 1.617 Å, $(K-O)_{inner}$ = $(K-O)_{outer}$ = 3.104 Å, and for Krivoi Rog α = 0.5º, Δz = 0.032 Å, <Si,Al−O> = 1.617 Å, $(K-O)_{inner}$ = 3.084, $(K-O)_{outer}$ = 3.107 Å. Thus, in both celadonite structures, tetrahedral rings are nearly hexagonal and the interlayer cation resides in a regular hexagonal prism. Tetrahedral cations and basal oxygen atoms of adjacent tetrahedral sheets are almost superimposed along the *c** axis. The small α and Δz values, along with limited Al substitution in the tetrahedral sheets, are characteristic of the celadonite structure. Hence, as discussed above, the preferences for 2*n*60º by ditrigonal symmetry and for ±60º or ±120º by a Δz value are not expected in the structure and all

https://doi.org/10.1346/CCMN.2008.0560602 Published online by Cambridge University Press

rotation angles may occur equally. However, as described above, the celadonite specimens contain only 180º rotation as stacking faults in the 1*M* stacking.

One of the possible factors responsible for the absence of ±60º and ±120º stacking rotation in celadonite may be related to the lateral periodicity of the layers. For example, if $b/a \neq \sqrt{3}$, both rotated (except 180º) and non-rotated layers have a different orthogonal unit cell. Thus, the two-dimensional (2D) periodicities within the rotated layer pair will be non-commensurate. To adjust to a common 2D periodicity, the structure of the rotated layers will be modified slightly creating a certain strain which may restrict the occurrence of stacking faults with ±60º or ±120º rotation. However, in the studied samples, *b*/*a* is 1.731 for Taiheizan and 1.727 for Zaval'e (Table 1). These values are so close to $\sqrt{3}$ that the stacking faults with ±60º or ±120º rotation will not interfere with 2D periodicity of the stacking sequence.

The relationship between stacking sequence and ribbon-like morphology of celadonite

Zhukhlistov *et al.* (1979) reported the occurrence of two types of celadonite crystals with different morphologies from Krivoi Rog. One has a plate-like shape, which was formed by metasomatic reaction from Fe-rich biotite. Another has a large ribbon-like shape, which grew in an empty space by direct crystallization in solution. They are similar in chemical composition and cell dimensions, but OTED indicated that the stacking of the plate-like crystals is more disordered than the ribbon-like crystals. Zhukhlistov *et al*. (1977) and Zhukhlistov (2005) used the latter type for the structure analysis by OTED and the present study also investigated this type. The result of Zhukhlistov *et al.* (1979) suggests that the stacking feature of celadonite is significantly influenced by the condition during crystal growth.

Güven (2001) considered the relationships between the morphological features of *trans*-vacant (*tv*) 1*M* mica crystallites and the relative growth rates along different lateral directions within the mica layer. He concluded that a pseudo-hexagonal plate-like habit of the *tv* 1*M* crystal develops when the growth rates are equal on the (010), (110), and ($\bar{1}$10) fronts, and that laths or fibers develop when the growth rate on the (010) fronts is slower than on the (110) and ($\bar{1}$10) fronts. He showed that the atomic configurations exposed on the (010), (110), and ($\bar{1}$10) planes are different: the (010) plane exposes pairs of octahedral OH groups whereas the (110) and ($\bar{1}$10) planes expose octahedral *cis*-sites occupied by cations and numerous broken bonds (Güven, 2001). The (110) and ($\bar{1}$10) fronts are therefore expected to grow faster than the (010) fronts, resulting in laths or fibers with their longest dimensions parallel to the *a* axis. According to Güven (2001), not only the crystal but the *tv* 2:1 unit layer itself also has such a growth character. This was also confirmed experimentally by Baronnet *et al*. (1976). Crystallites are expected in which constituent *tv* 2:1 layers have parallel (1*M* stacking) or antiparallel (180º layer rotation) orientations which can grow more rapidly than those containing layers with ±60º and/or ±120º layer rotations. As a consequence, the crystals with 1*M* and only 180º stacking faults may occupy larger volumes than those containing ±60º and/or ±120º stacking faults in the specimen. This is illustrated in Figure 5. Suppose, for example, that several new layers with various orientations are nucleating on a crystal with a ribbon-like form. These new layers are also assumed to have the ability to elongate along the *a* axis (note that this is the axis for the two-dimensional unit layer), as mentioned above. In this situation, new layers with ±60º or ±120º rotations (the left one) expand on the preceding layer along the *a* axis but soon reach the side-end of the ribbon-like crystal. Then, growth occurs only on the (010) fronts and becomes very slow. On the other hand, new layers with 0º and 180º (the right one) can expand more widely owing to the parallelism with the preceding layer or crystal. As a consequence, the latter is dominant on the crystal and a large portion of the crystal has stacking with 0º (1*M* stacking) and 180º layer rotation. Such a quantitative dominance may be reflected in the XRD and HRTEM results in the present investigation.

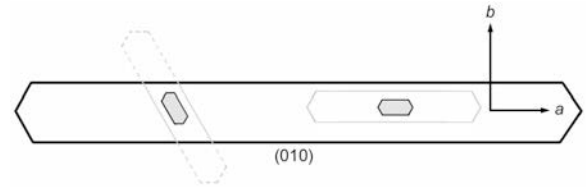

Figure 5. A model to show limited (left) and unlimited (right) layer growth of nuclei with (±60º, ±120º) and (0º, 180º) layer rotations, respectively, on a ribbon-like crystal. See the text for details.

The morphology of illite has been shown experimentally to be influenced considerably by the growth conditions (Güven, 2001), and can thus affect the dominant stacking sequence through the change of morphology. For example, glauconite has a similar composition to celadonite except that it is deficient in interlayer cations (Rieder *et al*., 1999). Glauconite often occurs in marine sediments and its crystallites grow very slowly by direct precipitation at low temperature in diagenetic environments (Odom, 1984). Under such conditions, *tv* 2:1 layers may grow with a plate-like form rather than a ribbon-like form. Sakharov *et al*. (1990) noted that stacking faults involving 2*n*60º and (2*n*+1)60º layer rotations occur with equal probability in galuconite, and these can be attributed to the plate-like form of the *tv* 2:1 layers in such growth environments.

ACKNOWLEDGMENTS

The authors are grateful to S. Guggenheim for helpful discussions and improvement of the English. They also thank A. Baronnet, G. Ferarris, and M.F. Brigatti for their

https://doi.org/10.1346/CCMN.2008.0560602 Published online by Cambridge University Press

valuable comments which helped to improve the manuscript significantly. This work was partly supported by a Grant-in-Aid No. 17340160 [Section (B)] from the Japan Society for the Promotion of Science (JSPS). JK was supported financially by a JSPS Research Fellowship for Young Scientists. VD thanks the Russian Foundation for Basic Research for support.

REFERENCES

Bailey, S.W. (1984) Classification and structures of the micas. Pp. 1–12 in: *Micas* (S.W. Bailey, editor). Reviews in Mineralogy, **13**. Mineralogical Society of America, Washington, D.C.

Baronnet, A. (1992) Polytypism and stacking disorder. Pp. 231–282 in: *Minerals and Reactions at the Atomic Scale: Transmission Electron Microscopy* (P.R. Buseck, editor). Reviews in Mineralogy, **27**, Mineralogical Society of America, Washington, D.C.

Baronnet, A., Amouric, M., and Chabot, B. (1976) Méchanismes de croissance, polytypisme et polymorphisme de la muscovite hydroxylée synthétique. *Journal of Crystal Growth*, **32**, 37–59 (in French with English abstract).

Baronnet, A. and Kang, Z.C. (1989) About the origin of mica polytypes. *Phase Transitions*, **16/17**, 477–493.

Brigatti, M.F., Caprilli, E., Malferrari, D., Medici, L., and Poppi, L. (2005) Crystal structure and chemistry of trilithionite-2M_2 and polylithionite-2M_2. *European Journal of Mineralogy*, **17**, 475–481.

Brigatti, M.F., Frigieri, P., and Poppi, L. (1998) Crystal chemistry of Mg-, Fe-bearing muscovite-2M_1. *American Mineralogist*, **83**, 775–785.

Brigatti, M.F. and Guggenheim S. (2002) Mica crystal chemistry and the influence of pressure, temperature and solid solution on atomistic models. Pp. 1–97 in: *Micas: Crystal Chemistry and Metamorphic Petrology* (A. Mottana, F.E. Sassi, J.B. Thompson Jr., and S. Guggenheim, editor). *Reviews in Mineralogy and Geochemistry*, **46**, Mineralogical Society of America, and the Geochemical Society, Washington, D.C.

Buckley, H.A., Bevan, J.C., Brown, K.M., and Johnson, L.R. (1978) Glauconite and celadonite: two separate mineral species. *Mineralogical Magazine*, **42**, 373–382.

Cuadros, J. and Altaner, S.P. (1998a) Characterization of mixed-layer illite-smectite from bentonites using microscopic, chemical and X-ray methods: constraints on the smectite-to-illite transformation mechanism. *American Mineralogist*, **83**, 762–774.

Cuadros, J. and Altaner, S.P. (1998b) Compositional and structural features of the octahedral sheet in mixed-layer illite-smectite from bentonites. *European Journal of Mineralogy*, **10**, 111–124.

Drits, V.A., Besson, G., and Muller, F. (1995) An improved model for structural transformations of heat-treated aluminous dioctahedral 2:1 layer silicates. *Clays and Clay Minerals*, **43**, 718–731.

Drits, V.A., McCarty, D.K., and Zviagina, B.B. (2006) Crystal-chemical factors responsible for the distribution of octahedral cations over *trans*- and *cis*-sites in dioctahedral 2:1 layer silicates. *Clays and Clay Minerals*, **54**, 131–152.

Drits, V.A. and Tchoubar, C. (1990) *X-ray Diffraction of Disordered Lamellar Structures. Theory and Application to Microdivided Silicates and Carbons*. Springer Verlag, Berlin, 242 pp.

Drits, V.A., Zvyagin, B.B., and Tokmakov, P.P. (1966) Gümbelite – dioctahedral micas 2M_2. *Doklady Academii Nauk SSSR*, **170**, 1390–1394 (in Russian).

Ferraris, G., Gula, A., Ivaldi, G., Nespolo, M., Sokolova, E., Uvarova, Y., and Khomyakov, A.P. (2001) First structure determination of an MDO-2*O* mica polytype associated with a 1*M* polytype. *European Journal of Mineralogy*, **13**, 1013–1023.

Ferraris, G. and Ivaldi, G. (2002) Structural features of micas. Pp. 117–148 in: *Micas: Crystal Chemistry and Metamorphic Petrology* (A. Mottana, F.E. Sassi, J.B. Thompson Jr. and S. Guggenheim, editors). Reviews in Mineralogy and Geochemistry, **46**, Mineralogical Society of America and the Geochemical Society, Washington, D.C.

Giuseppetti, G. and Tadani, C. (1972) The crystal structure of 2*O* brittle mica: anandite. *Tschermaks Mineralogische und Petrographische Mitteilungen*, **18**, 169–184.

Güven, N. (2001) Mica structure and fibrous growth of illite. *Clays and Clay Minerals*, **49**, 189–196.

Iijima, S. and Buseck, P.R. (1978) Experimental study of disordered mica structures by high-resolution electron microscopy. *Acta Crystallographica*, **A34**, 709–719.

Kameda, J., Miyawaki, R., Drits, V.A., and Kogure, T. (2007) Polytype and morphological analyses of gümbelite, a fibrous Mg-rich illite. *Clays and Clay Minerals*, **55**, 453–466.

Kilaas, R. (1998) Optimal and near-optimal filters in high-resolution electron microscopy. *Journal of Microscopy*, **190**, 45–51.

Kimbara, K. and Shimoda, S. (1973) A ferric celadonite in amygdales of dolerite at Taiheizan, Akita prefecture, Japan. *Clay Science*, **4**, 143–150.

Kogure, T. (2002) Investigation of micas using advanced TEM. Pp. 281–310 in: *Micas: Crystal Chemistry & Metamorphic Petrology* (A. Mottana, F.P. Sassi, J.B. Thompson, Jr. and S. Guggenheim, editors). Reviews in Mineralogy and Geochemistry, **46**, Mineralogical Society of America and the Geochemical Society, Washington, D.C.

Kogure, T. (2007) Imaging of dioctahedral 2:1 layers by high-resolution transmission electron microscopy (HRTEM): Possibility of recording the dehydroxylate. *American Mineralogist*, **92**, 1368–1373.

Kogure, T. and Bunno, M. (2004) Investigation of polytype in lepidolite using electron back-scattered diffraction. *American Mineralogist*, **89**, 1680–1684.

Kogure, T., Jige, M., Kameda, J., Yamagishi, A., and Kitagawa, R. (2006) Stacking structures in pyrophyllite revealed by high-resolution transmission electron microscopy (HRTEM). *American Mineralogist*, **91**, 1293–1299.

Kogure, T., Kameda, J., and Drits, V.A. (2007) Novel 2:1 structure of phyllosilicates formed by annealing Fe^{3+}, Mg-rich dioctahedral micas. *American Mineralogist*, **92**, 1531–1534.

Kogure, T. and Nespolo, M. (1999a) First finding of a stacking sequence with (±60º, 180º) rotation in biotite. *Clays and Clay Minerals*, **47**, 784–792.

Kogure, T. and Nespolo, M. (1999b) A TEM study of long-period mica polytypes: determination of the stacking sequence of oxybiotite by means of atomic-resolution images and Periodic Intensity Distribution (PID). *Acta Crystallographica*, **B55**, 507–516.

Levinson, A.A. (1953) Studies in the mica group; Relationship between polymorphism and composition in the muscovite–lepidolite series. *American Mineralogist*, **38**, 88–107.

Malkova, K.M. (1956) Celadonite from Pobuj'e. *Mineralogicheski sbornik L'vovskogo. Mineralogicheskogo Obtchestva*, **10**, 305–318 (in Russian).

Marks, L.D. (1996) Wiener-filter enhancement of noisy HREM images. *Ultramicroscopy*, **62**, 43–52.

McCarty, D.K. and Reynolds, R.C. Jr. (1995) Rotationally disordered illite-smectite in Paleozoic K-bentonites. *Clays and Clay Minerals*, **43**, 271–284.

Muller, F., Drits, V.A., Plançon, A., and Robert, J.-L. (2000a) Structural transformation of 2:1 dioctahedral layer silicates during dehydroxylation-rehydroxylation reactions. *Clays*

and Clay Minerals, **48**, 572–585.

Muller, F., Drits, V.A., Plançon, A., and Besson, G. (2000b) Dehydroxylation of Fe^{3+}, Mg-rich dioctahedral micas: (I) structural transformation. *Clay Minerals*, **35**, 491–504.

Odom, I.E. (1984) Glauconite and celadonite minerals. Pp. 545–572 in: *Micas* (S.W. Bailey, editor). Reviews in Mineralogy, **13**, Mineralogical Society of America, Washington, D.C.

Rieder, M., Cavazzini, G., D'yakonov, Yu.S., Frank-Kamenetskii, V.A., Gottardi, G., Guggenheim, S., Koval', P.V., Müller, G., Neiva, A.M.R., Radoslowich, E.W., Robert, J.L., Sassi, F.P., Takeda, H., Weiss, Z., and Wones, D.R. (1999) Nomenclature of the micas. *Mineralogical Magazine*, **63**, 267–279.

Sakharov, B.A., Besson, G., Drits, V.A., Kameneva, M.Yu., Salyn, A.L., and Smoliar, B.B. (1990) X-ray study of the nature of stacking faults in the structure of glauconites. *Clay Minerals*, **25**, 419–435.

Slonimskaya, M.V., Drits, V.A., Finko, V.I., and Salyn, A.L. (1978) The nature of interlayer water in fine-dispersed muscovites. *Izvestiya Akademii Nauk SSSR*, *Seriya Geologicheskaya*, **10**, 95–104 (in Russian).

Takeda, H., Haga, N., and Sadanaga, R. (1971) Structural investigation of a polymorphic transition between $2M_2$-, $1M$-lepidolite and $2M_1$-muscovite. *Mineralogical Journal*, **6**, 203–215.

Threadgold, I.M. (1959) A hydromuscovite with the $2M_2$ structure, from Mount Lyell, Tasmania. *American Mineralogist*, **44**, 488–494.

Treacy, M.M.J., Newsam, J.M., and Deem, M.W. (1991) A general recursion method for calculating diffracted intensities from crystals containing planar faults. *Proceedings of the Royal Society of London A*, **433**, 499–520.

Tsipursky, S.I., Kameneva, M.Y., and Drits, V.A. (1985) Structural transformation of Fe^{3+}-conatining 2:1 dioctahedral phyllosilicates in the course of dehydroxylation. Pp. 567–577 in: *5th meeting of the European Clay Groups* (J. Konta, editor). Prague.

Tsipursky, S.I. and Drits, V.A. (1986) Refinement of celadonite crystal structure. *Mineralogical Journal*, **8**, 32–40 (in Russian).

Ylagan, R.F., Altaner, S.P., and Pozzuoli, A. (2000) Reaction mechanisms of smectite illitization associated with hydrothermal alteration from Ponza island, Italy. *Clays and Clay Minerals*, **48**, 610–631.

Zhukhlistov, A.P. (2005) Crystal structure of celadonite from the electron diffraction data. *Crystallography Reports*, **50**, 902–906.

Zhukhlistov, A.P., Zviagin, B.B., Lazarenko, E.K., and Pavlishin, V.I. (1977) Refinement of α iron celadonite structure. *Kristallographya*, **22**, 498–505 (in Russian) [*Soviet Physics and Crystallography*, **22**, 284–290].

Zhukhlistov, A.P., Zviagin, B.B., Lazarenko, E.K., and Pavlishin, V.I. (1979) Typomorphic features of celadonite structure. *Zapiski Vsesouznogo Mineralogicheskogo Obtchestva*, **108**, 348–353.

Zhukhlistov, A.P., Zviagin, B.B., Soboleva, S.V., and Fedotov, A.F. (1973) The crystal structure of the dioctahedral mica $2M_2$ determined by high voltage electron diffraction. *Clays and Clay Minerals*, **21**, 465–470.

(*Received 14 March 2008; revised 9 August 2008; Ms. 0139; A.E. B. Lanson*)